TIME DOMAIN RADIAL FILTER DESIGN FOR SPHERICAL WAVES

Nara Hahn, Frank Schultz, and Sascha Spors

Institute of Communications Engineering
University of Rostock, 18119 Rostock, Germany

ABSTRACT

Signal processing based on spherical harmonic representations requires an efficient and accurate modeling of the radial functions whose spectrum is commonly described by spherical Bessel and Hankel functions. In this paper, the time-domain radial functions for spherical waves are realized as FIR filters. The filter design exploits the continuous-time representations of the radial functions which have a finite temporal support and are described by the Legendre polynomials. Since the discontinuities occurring in the time domain exhibit infinite temporal bandwidth, a direct time-domain sampling results in frequency-domain aliasing. In order to reduce the aliasing artifacts, the time-domain discontinuities of different orders are replaced with band-limited functions that are analytically derived from the Lagrange interpolation kernel. The FIR coefficients are then obtained by sampling the band-limited representations which leads to a considerable reduction in spectral aliasing. The coefficients are given in closed form expressed solely by polynomials which makes the proposed method suited for real-time applications.

***Index Terms*—** Radial filter, radial function, spherical harmonic expansion, spherical wave

1. INTRODUCTION

Sound field control techniques such as spatial sound reproduction and active noise control commonly rely on analytical representations of sound fields. Traditionally, spherical harmonic expansion has mainly been used for configurations with spherical symmetries [1, 2, 3, 4]. It has gained increasing attention in spatial sound recording and reproduction due to its direction-independent spatial resolution [5]. Spherical/cylindrical harmonic representations are also used in local sound field synthesis where the desired sound field within a local region is described with a finite modal bandwidth [6, 7, 8].

In practice, modeling and manipulation of spherical harmonic signals require the discretization of the radial basis functions. Sampling the radial functions in the frequency domain is computationally demanding, since the spherical Bessel/Hankel functions have to be evaluated at all frequency bins. Moreover, the resulting impulse response typically exhibits long transients due to the limited temporal bandwidth and time-domain aliasing. As an alternative approach, time-domain design of the radial functions has been addressed where the radial functions are realized as digital filters. The filter type is chosen based on the spatio-temporal structure of the sound field. While singular radial functions are commonly modeled by infinite impulse response (IIR) filters [9, 10, 11], regular radial functions are usually modeled by finite impulse response (FIR) filters [12, 13, 14, 15]. In the latter case, the FIR coefficients are obtained from the time-domain representations of the radial functions which are typically described by Legendre polynomials [16, 17].

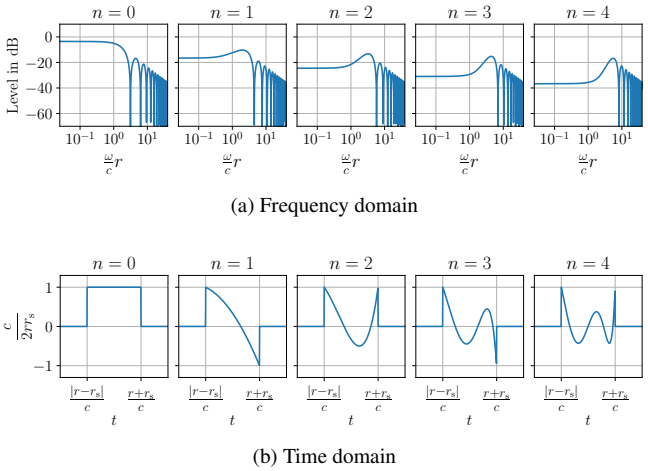

(a) Frequency domain

(b) Time domain

Fig. 1: Radial functions for a spherical wave ($r = 1\,\mathrm{m}$, $r_\mathrm{s} = 1.5\,\mathrm{m}$).

Although the design of the FIR radial filters can be carried out efficiently by directly sampling the continuous-time radial functions, the resulting spectral accuracy is often impaired due to aliasing artifacts [18]. These are mainly attributed to the discontinuities occurring in the time domain which exhibit an infinite bandwidth. An improved time-domain modeling was introduced for plane-wave radial functions in [19, 20], where an analytical anti-aliasing filtering is applied to the continuous-time representations. The time-domain discontinuities are replaced with the anti-derivatives of a prototype low-pass filter whose impulse response is described by interpolation polynomials [21, 22, 23]. It was shown to be effective in reducing the aliasing distortion while preserving the temporal compactness of the original radial functions [20].

In this study, we extend this method to the radial functions for spherical waves. The temporal and spectral properties of the spherical-wave radial functions are investigated in Sec. 2. Section 3 presents the proposed radial filter design which is based on the higher-order discontinuities of the time-domain radial functions. The validity of the proposed radial filter design is evaluated by numerical results in Sec. 4.

2. RADIAL FUNCTIONS

This section reviews the spherical harmonic representations of spherical waves. We pay particular attention to the radially-dependent parts which describe the spectral and temporal characteristics of the sound field. The observation point will be represented with spherical coordinates $\boldsymbol{x} = (r, \theta, \phi)$ where r denotes the radius, θ the colatitude and ϕ the azimuth. It is assumed that an ideal point source is

located at $\boldsymbol{x}_\mathrm{s} = (r_\mathrm{s}, \theta_\mathrm{s}, \phi_\mathrm{s})$ emitting a spherical wave in a free field.

The spherical wave driven with a harmonic signal can be expanded as [1, Eq. (8.22)]

$$\frac{e^{-i\frac{\omega}{c}R}}{4\pi R} = \sum_{n=0}^{\infty} \frac{2n+1}{4\pi} (-i\tfrac{\omega}{c}) j_n(\tfrac{\omega}{c} r_\vee) h_n(\tfrac{\omega}{c} r_\wedge) P_n(\cos\Theta_\mathrm{s}), \quad (1)$$

where $j_n(\cdot)$ denotes the spherical Bessel function of the first kind, $h_n(\cdot)$ the spherical Hankel function of the second kind, and $P_n(\cdot)$ the Legendre polynomial. The non-negative integer n denotes the spherical harmonic order. The Euclidean distance between $\boldsymbol{x}$ and $\boldsymbol{x}_\mathrm{s}$ is denoted by R. The radial variables $r_\vee$ and $r_\wedge$ are respectively defined as the smaller and greater in $\{r, r_\mathrm{s}\}$. Since the sound field is axis-symmetric with respect to $\boldsymbol{x}_\mathrm{s}$, the directional dependency is represented by the angle between $\boldsymbol{x}$ and $\boldsymbol{x}_\mathrm{s}$ denoted by Θ_s. The angular frequency ω is related to the frequency f by $\omega = 2\pi f$. The speed of sound is denoted by c and the imaginary unit by i. The time harmonic term $e^{i\omega t}$ is omitted for brevity.

In (1), the radial and frequency dependencies of each order are described by the so-called radial function $-i\frac{\omega}{c}\, j_n(\frac{\omega}{c} r_\vee)\, h_n(\frac{\omega}{c} r_\wedge)$. Exemplary magnitude spectra are depicted in Fig. 1(a). The notches and the decay at high frequencies ($\frac{\omega}{c} r_\vee > n$) are dominated by the spherical Bessel functions. For $n \geq 1$, the nth-order zeros of $j_n(\frac{\omega}{c} r_\vee)$ at $\omega = 0$ are canceled by the nth-order poles exhibited by $-i\frac{\omega}{c} h_n(\frac{\omega}{c} r_\wedge)$. As $\omega \to 0$, the magnitude response converges to $\frac{1}{2n+1}(r_\vee^n / r_\wedge^{n+1})$ which follows from the small argument approximations of $j_n(\cdot)$ and $h_n(\cdot)$ [24, Eq. (10.52.1) and (10.52.2)]. A more thorough discussion on the radial functions can be found in [18].

The time-domain expression of the spherical wave excited by a Dirac delta function $\delta(t)$ reads [12, 16, 25]

$$\frac{\delta(t - \frac{R}{c})}{4\pi R} = \sum_{n=0}^{\infty} \frac{2n+1}{4\pi} \frac{c}{2 r r_\mathrm{s}} \tilde{P}_n\left(\frac{r^2 + r_\mathrm{s}^2 - (ct)^2}{2 r r_\mathrm{s}}\right) P_n(\cos\Theta_\mathrm{s}). \quad (2)$$

The function $\tilde{P}_n(\cdot)$ is the Legendre polynomials if the argument is smaller than unity in magnitude, and equals zero elsewhere. For the sake of brevity, the argument will be denoted by $\gamma_t = \frac{r^2 + r_\mathrm{s}^2 - (ct)^2}{2 r r_\mathrm{s}}$. As depicted in Fig. 1(b), the time-domain radial functions $\frac{c}{2 r r_\mathrm{s}} \tilde{P}_n(\gamma_t)$ have a finite support $\frac{|r - r_\mathrm{s}|}{c} < t < \frac{r + r_\mathrm{s}}{c}$, where the onset and offset $t = \frac{|r \mp r_\mathrm{s}|}{c}$ correspond to $\gamma_t = \pm 1$.

In practice, the infinite series expansions, (1) and (2), are typically truncated to finite sums ($n = 0, \ldots, N$). This is referred to as spatial band limitation where the maximum harmonic order N is the spatial bandwidth. A spatially band-limited expansion is suited for the approximation of a sound field at low frequencies ($f < \frac{cN}{2\pi r}$) or in the neighborhood of the expansion center ($r < \frac{cN}{2\pi f}$) [2, Ch. 9]. Figure 2 shows the snapshots of a spatially band-limited ($N = 20$) spherical wave (2). It can be interpreted as a superposition of sound fields emitted by continuously distributed point sources on the sphere $r = r_\mathrm{s}$. The strength of the individual sources is proportional to the angular dependent term $P_n(\cos\Theta_\mathrm{s})$.

3. RADIAL FILTER DESIGN

This section presents an FIR design of the spherical-wave radial filters which is based on the time-domain representation (2). The radial filters obtained by directly sampling (2) are susceptible to aliasing distortions since the original spectrum is not band limited (cf. Fig. 1(a)). The waveform of the time-domain radial functions

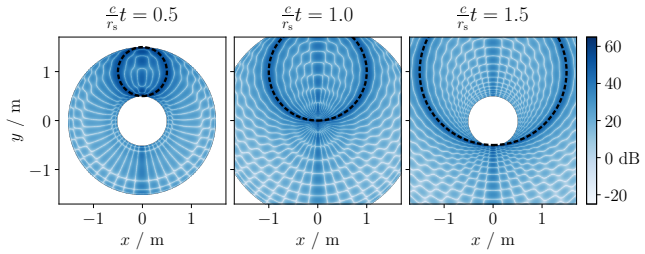

Fig. 2: Snapshots ($\frac{c}{r_\mathrm{s}} t = 0.5, 1.0, 1.5$, xy-plane) of a spatially band-limited spherical wave (point source at $\boldsymbol{x}_\mathrm{s} = (1, \frac{\pi}{2}, \frac{\pi}{2})$, spatial bandwidth $N = 20$). The dashed lines indicate the spherical wavefront of the original sound field without spatial band-limitation ($N \to \infty$).

(cf. Fig. 1(b)) suggests that the high-frequency components mainly result from the discontinuities occurring at $|\gamma_t| = 1$. This not only concerns the jump discontinuities (zeroth-order) but also the discontinuities of the high-order derivatives with respect to t.

3.1. Discontinuities

The discontinuities occurring in the time domain are examined by comparing the derivatives of the radial functions for $|\gamma_t| > 1$ and $|\gamma_t| < 1$. It is apparent that the derivatives for $|\gamma_t| > 1$ are zero,

$$\tfrac{\mathrm{d}^k}{\mathrm{d}t^k} \big[\tilde{P}_n(\gamma_t)\big]_{|\gamma_t|>1} = 0, \quad k = 0, 1, \ldots \quad (3)$$

where k denotes the derivative order. The amplitude $\frac{c}{2 r r_\mathrm{s}}$ is dropped for brevity. The derivatives for $|\gamma_t| < 1$ reads

$$\tfrac{\mathrm{d}^k}{\mathrm{d}t^k} \big[\tilde{P}_n(\gamma_t)\big]_{|\gamma_t|<1} \quad (4)$$
$$= \begin{cases} \sum_{l=\lceil \frac{k}{2} \rceil}^{\min\{k,n\}} \alpha_{k,l} P_n^{(l)}(\gamma_t) \big(-\tfrac{c^2}{r r_\mathrm{s}}\big)^l t^{2l-k}, & k = 0, \ldots, 2n \\ 0, & k = 2n+1, \ldots \end{cases}$$

which follows from the Faá di Bruno's formula [26]. The lth derivative of the Legendre polynomial is denoted by $P_n^{(l)}(\cdot)$. The coefficients defined as $\alpha_{k,l} = \frac{k!}{(2l-k)!(k-l)!2^{k-l}}$ can be computed recursively in descending order by exploiting $\alpha_{k,k} = 1$ and

$$\alpha_{k,l-1} = \frac{(2l-k-1)(2l-k)}{2(k-l+1)}\, \alpha_{k,l}. \quad (5)$$

A detailed derivation of (4) is given in the Appendix (Sec. 6).

We define the kth-order discontinuity at a given point as the difference between the left and right limits of the kth derivative,

$$\eta_n^{(k)}(t) \coloneqq \lim_{\epsilon \to 0} \Big(\tfrac{\mathrm{d}^k}{\mathrm{d}t^k} \big[\tilde{P}_n(\gamma_t)\big]_{t+\epsilon} - \tfrac{\mathrm{d}^k}{\mathrm{d}t^k} \big[\tilde{P}_n(\gamma_t)\big]_{t-\epsilon} \Big). \quad (6)$$

Substituting (3) and (4) into (6) and evaluating at $t = \frac{|r \mp r_\mathrm{s}|}{c}$ yields

$$\eta_n^{(k)}\big(\tfrac{|r \mp r_\mathrm{s}|}{c}\big) = \pm \tfrac{\mathrm{d}^k}{\mathrm{d}t^k} \big[P_n(\gamma_t)\big]_{\gamma_t = \pm 1} \quad (7)$$
$$= \pm \big(\tfrac{c}{|r \mp r_\mathrm{s}|}\big)^k \sum_{l=\lceil \frac{k}{2} \rceil}^{\min\{k,n\}} \alpha_{k,l} P_n^{(l)}(\pm 1) \big(\pm 2 - \tfrac{r}{r_\mathrm{s}} - \tfrac{r_\mathrm{s}}{r}\big)^l.$$

The radial functions can be represented as a superposition of two right-sided functions [17, 20],

$$\tilde{P}_n(\gamma_t) = \sum_{k=0}^{2n} \Big[\eta_n^{(k)}(\tfrac{|r-r_\mathrm{s}|}{c}) \tfrac{1}{k!} \big(t - \tfrac{|r-r_\mathrm{s}|}{c}\big)^k u\big(t - \tfrac{|r-r_\mathrm{s}|}{c}\big) + \eta_n^{(k)}(\tfrac{r+r_\mathrm{s}}{c}) \tfrac{1}{k!} \big(t - \tfrac{r+r_\mathrm{s}}{c}\big)^k u\big(t - \tfrac{r+r_\mathrm{s}}{c}\big) \Big], \quad (8)$$

with $u(\cdot)$ denoting the Heaviside step function. The right-sided functions are described by the Taylor series expansions about $t = \frac{|r \mp r_\mathrm{s}|}{c}$. Note that the maximum discontinuity order ($2n$) of the spherical-wave radial functions is twice as high as for the plane-wave radial functions [20, Eq. (27)].

3.2. Band Limitation

In (8), the kth-order discontinuity is described in the form of $\frac{1}{k!}(t-\tau)^k u(t-\tau)$. This corresponds to the kth-order anti-derivative of the delayed Dirac delta function $\delta(t-\tau)$ [20, Sec. 3],

$$F_0(t-\tau) = \int_{-\infty}^{t} \delta(t'-\tau)\mathrm{d}t' = u(t-\tau) \quad (9)$$

$$F_k(t-\tau) = \int_{-\infty}^{t} F_{k-1}(t'-\tau)\mathrm{d}t' = \frac{(t-\tau)^k}{k!} u(t-\tau). \quad (10)$$

In the proposed radial filter design, a temporal band limitation is applied to the discontinuity functions $F_k(t-\tau)$ by replacing $\delta(t)$ with the impulse response of a low-pass filter $h(t)$ [21, 22, 23], yielding

$$H_0(t-\tau) = \int_{-\infty}^{t} h(t'-\tau)\mathrm{d}t' \quad (11)$$

$$H_k(t-\tau) = \int_{-\infty}^{t} H_{k-1}(t'-\tau)\mathrm{d}t'. \quad (12)$$

The low-pass filtered radial functions can thus be written as

$$\begin{aligned} &h(t) *_t \tilde{P}_n(\gamma_t) \\ &= \sum_{k=0}^{2n} \Big[\eta_n^{(k)}(\tfrac{|r-r_\mathrm{s}|}{c}) H_k\big(t - \tfrac{|r-r_\mathrm{s}|}{c}\big) + \eta_n^{(k)}(\tfrac{r+r_\mathrm{s}}{c}) H_k\big(t - \tfrac{r+r_\mathrm{s}}{c}\big) \Big] \\ &= \tilde{P}_n(\gamma_t) + \sum_{k=0}^{2n} \Big[\eta_n^{(k)}(\tfrac{|r-r_\mathrm{s}|}{c}) D_k\big(t - \tfrac{|r-r_\mathrm{s}|}{c}\big) + \eta_n^{(k)}(\tfrac{r+r_\mathrm{s}}{c}) D_k\big(t - \tfrac{r+r_\mathrm{s}}{c}\big) \Big], \end{aligned} \quad (13)$$

where $D_k(t-\tau) := H_k(t-\tau) - \frac{1}{k!}(t-\tau)^k u(t-\tau)$ is called the residual function. Equation (13) states that the band limitation can be performed by superimposing the weighted residual functions $D_k(t-\tau)$ onto the original radial function. Note that the amplitude $\frac{c}{2 r r_\mathrm{s}}$ is omitted in (8) and (13) for brevity.

3.3. Prototype Filter

In this paper, we use the Lagrange interpolation kernel as the prototype low-pass filter $h(t)$. The impulse response is described by Mth-order polynomials (M: odd) within $M+1$ adjacent intervals defined by $M+2$ uniformly distributed nodes [27],

$$h(t) = \frac{\prod_{\nu=\mu-\frac{M-1}{2},\nu\neq 0}^{\mu+\frac{M+1}{2}} \left(\frac{t}{T_\mathrm{s}} - \nu\right)}{\big(\frac{M-1}{2}-\mu\big)!\big(\frac{M+1}{2}+\mu\big)!(-1)^{(\frac{M+1}{2}+\mu)}}, \quad (14)$$

for $\frac{t}{T_\mathrm{s}} \in [\mu, \mu+1]$ with $\mu = -\frac{M+1}{2}, \ldots, \frac{M-1}{2}$. The sampling period is denoted by T_s. The band-limited discontinuities $H_k(t)$ are obtained by evaluating the anti-derivatives of $h(t)$ (cf. (12)). The integration constants have to be chosen in such a way that the functions are continuous at the nodes [20, 21]. Also, the values at the outermost nodes have to match with the corresponding discontinuity functions,

$$H_k(-\tfrac{M+1}{2}T_\mathrm{s}) = 0 \quad \text{and} \quad H_k(\tfrac{M+1}{2}T_\mathrm{s}) = \tfrac{1}{k!}(\tfrac{M+1}{2}T_\mathrm{s})^k. \quad (15)$$

Due to the maximally flatness of the Lagrange interpolator [28, Sec. 3.3], the anti-derivatives and the corresponding residual functions can be derived up to order $K = M$. Note that a higher-order Lagrange polynomial is required to cope with higher-order discontinuities, which in turn increases the FIR length.

3.4. Sampling

The FIR coefficients of the radial filters are obtained by uniformly sampling the low-pass filtered expression (13). Due to the limited temporal bandwidth, the resulting filter will exhibit reduced aliasing distortions. The filter design can be carried out efficiently since the band-limited radial functions are fully described by polynomials (Legendre and Lagrange) and physical variables (i.e. r, r_s, c). Equation (13) suggests that the band limitation can be performed by first sampling the full-band radial functions (without band limitation) and then adding the sampled residual functions. Since the residuals $D_k(t)$ have a finite support, only a finite number of samples have to be modified around the discontinuities. For a given sampling frequency $f_\mathrm{s} := \frac{1}{T_\mathrm{s}}$, the FIR length is $L_\mathrm{FIR} = \lfloor \frac{r+r_\mathrm{s}}{c} f_\mathrm{s} \rfloor - \lceil \frac{|r-r_\mathrm{s}|}{c} f_\mathrm{s} \rceil + M + 2$ with $\lfloor\cdot\rfloor$ and $\lceil\cdot\rceil$ denoting the floor and ceiling functions, respectively.

4. EVALUATION

In this section, the spectral accuracy of the proposed approach is examined for different Lagrange polynomial orders M and anti-derivative orders K ($k = 0, \ldots, K$). The sampling frequency is set to $f_\mathrm{s} = 48\,\mathrm{kHz}$ and the speed of sound to $c = 343\,\mathrm{m/s}$.

The frequency responses of the radial filters $\hat{\mathcal{H}}_n(\omega)$ are compared with the exact spectra $\mathcal{H}_n(\omega) = (-i\frac{\omega}{c}) j_n(\frac{\omega}{c} r_\vee) h_n(\frac{\omega}{c} r_\wedge)$ from (1). Figure 3 depicts the spectral deviation defined as

$$\mathcal{E}_n(\omega) := 20 \log_{10} \Big(\big| \hat{\mathcal{H}}_n(\omega) - \mathcal{H}_n(\omega) \big| \Big)\,\mathrm{dB}. \quad (16)$$

Polynomial order $M = 5$ and varying anti-derivative orders K are considered. The results for the FIR radial filters without band limitation are also shown for comparison (— labeled as 'None'). It can be seen that the proposed approach achieves a considerable improvement even for $K = 0$ (—) where the band-limitation is only applied to the zeroth-order discontinuities. As n increases, higher anti-derivative orders are needed to achieve comparable results. For $K = 2n$, the spectral deviations at low frequencies ($< 100\,\mathrm{Hz}$ in this case) decreases down to the numerical precision. The increasing errors towards high frequencies are attributed to the non-ideal low-pass characteristics of the Lagrange interpolator. The slope of the spectral deviation $\mathcal{E}_n(\omega)$ in the neighborhood of $\frac{f_\mathrm{s}}{2}$ is found to be proportional to the polynomial order M (not shown here). The results for $n = 2$ shows that the frequency range benefiting from the band limitation largely depends on the anti-derivative order K. The band limitation of the zeroth-order discontinuity is most effective in

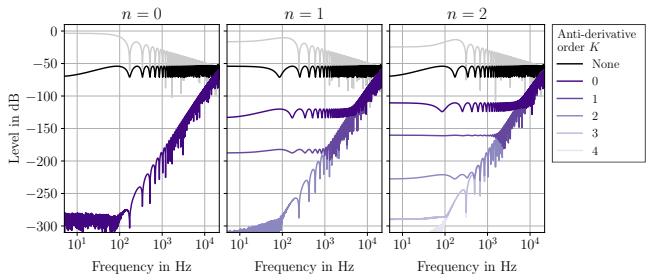

Fig. 3: Spectral deviations of the radial filters (harmonic order $n = 0, 1, 2$, Lagrange polynomial order $M = 5$, anti-derivative order $K = 0, \ldots, 2n$, $L_{\text{FIR}} = 286$, $r = 1\,\text{m}$, $r_\text{s} = 1.5\,\text{m}$, $f_\text{s} = 48\,\text{kHz}$). The results without band-limitation is indicated by black curves (—, $L_{\text{FIR}} = 280$). The gray curves (—) show the original spectra.

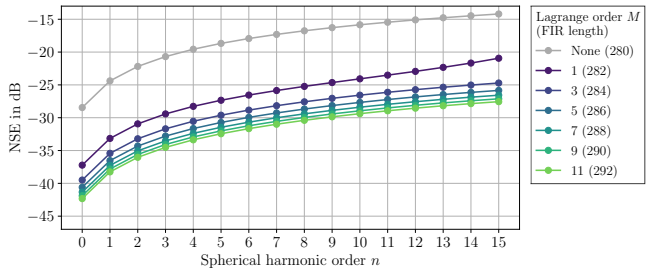

Fig. 4: Normalized squared error (17) of the radial filters (harmonic order $n = 0, \ldots, 15$, Lagrange polynomial order $M = 1, 3, \ldots, 11$, anti-derivative order $K = 2n$, $r = 1\,\text{m}$, $r_\text{s} = 1.5\,\text{m}$, $f_\text{s} = 48\,\text{kHz}$).

reducing aliasing, both in terms of bandwidth and energy. Higher-order anti-derivatives further reduce the aliasing artifacts but only within an increasingly narrow band.

The overall accuracy is evaluated in terms of the normalized squared error (NSE),

$$\text{NSE} \coloneqq 10 \log_{10} \left(\frac{\|\hat{\mathcal{H}}_n(\omega) - \mathcal{H}_n(\omega)\|^2}{\|\mathcal{H}_n(\omega)\|^2} \right) \text{dB}, \tag{17}$$

where $\|\cdot\|$ denotes the l_2-norm of the spectrum ($|\omega| < \pi f_\text{s}$) uniformly sampled at 2^{16} frequency bins. Figure 4 shows the results for varying polynomial orders M. In all cases, the maximum anti-derivative order is $K = \min\{2n, M\}$. It is shown again that even low-order polynomials are quite effective in improving the accuracy. Higher polynomial orders clearly reduces the aliasing artifacts but by a gradually diminishing degree. We found that, for each M, the norm of the spectral deviation (i.e. numerator in (17)) stays almost constant for varying n (not shown here), whereas the energy of the radial function (denominator) decreases approximately proportional to $\frac{1}{2n+1}$. This leads to the monotonic increase of the NSE.

5. CONCLUSION

The spherical harmonic expansion of spherical waves is modeled in the discrete-time domain where the radial and frequency-dependent terms (called radial functions) are realized as FIR filters. The FIR coefficients are derived from the band-limited representations of the radial filters. The aliasing distortions resulting from the higher-order discontinuities are reduced by applying a band-limitation using the anti-derivatives of the Lagrange interpolator. Since the argument of the radial functions is a quadratic function of time, the maximum discontinuity order is twice as high as for the plane-wave case. It was shown that the frequency-domain accuracy of the radial filters can be improved considerably by updating only a few samples around the discontinuities occurring in the time domain. Since all the relevant coefficients are represented by polynomials in analytical form, the filter coefficients can be computed efficiently. The proposed radial filter design is thus suited for the real-time implementation of sound field control techniques where the radial filters have to be updated instantly according to parameter changes.

6. APPENDIX: HIGHER-ORDER DERIVATIVES

The higher-order derivatives of the composite function $P_n\big(\gamma_t\big)$ can be expressed by using the Faá di Bruno's formula [26, 29],

$$\begin{aligned} &\tfrac{\mathrm{d}^k}{\mathrm{d}t^k} P_n\big(\gamma_t\big) \\ &= \sum \frac{k!}{j_1! j_2! \cdots j_k!} P_n^{(l)}\big(\gamma_t\big) \Big[\frac{{\gamma_t}^{(1)}}{1!}\Big]^{j_1} \Big[\frac{{\gamma_t}^{(2)}}{2!}\Big]^{j_2} \cdots \Big[\frac{{\gamma_t}^{(k)}(t)}{k!}\Big]^{j_k}, \end{aligned} \tag{18}$$

where the sum is over the combinations of non-negative integers $\{j_1, j_2, \ldots, j_k\}$ satisfying

$$j_1 + 2\, j_2 + 3\, j_3 + \ldots + k\, j_k = k. \tag{19}$$

The integer l is then given as

$$j_1 + j_2 + j_3 + \ldots + j_k = l. \tag{20}$$

Since the argument $\gamma_t = \frac{r^2 + r_\text{s}^2 - (ct)^2}{2 r r_\text{s}}$ is a quadratic function of t,

$${\gamma_t}^{(1)} = -\frac{c^2 t}{r r_\text{s}} \quad \text{and} \quad {\gamma_t}^{(2)} = -\frac{c^2}{r r_\text{s}}, \tag{21}$$

whereas ${\gamma_t}^{(k)} = 0$ for $k \geq 3$. The addend in (18) vanishes if $j_k \neq 0$ for any $k \geq 3$. Therefore, we only need to consider the cases where $j_3 = j_4 = \ldots = j_k = 0$ which simplifies (19) and (20) to

$$j_1 + 2 \cdot j_2 = k \quad \text{and} \quad j_1 + j_2 = l, \tag{22}$$

yielding

$$j_1 = 2l - k \quad \text{and} \quad j_2 = k - l. \tag{23}$$

Since j_1 and j_2 are non-negative integers, $l \leq k \leq 2l$ must hold. Also, considering that $P_n(\cdot)$ is an nth-order polynomial, the sum needs to be evaluated only for $l \leq n$. Equation (18) is rewritten as

$$\begin{aligned} &\tfrac{\mathrm{d}^k}{\mathrm{d}t^k} P_n\big(\gamma_t\big) \\ &= \sum_{l=\lceil \frac{k}{2} \rceil}^{\min\{k,n\}} \frac{k!}{(2l-k)!(k-l)!} P_n^{(l)}\big(\gamma_t\big) \Big[\frac{{\gamma_t}^{(1)}}{1!}\Big]^{2l-k} \Big[\frac{{\gamma_t}^{(2)}}{2!}\Big]^{k-l} \\ &= \sum_{l=\lceil \frac{k}{2} \rceil}^{\min\{k,n\}} \underbrace{\frac{k!}{(2l-k)!(k-l)!2^{k-l}}}_{\alpha_{k,l}} P_n^{(l)}\big(\gamma_t\big) \Big(-\frac{c^2}{r r_\text{s}}\Big)^l t^{2l-k}, \end{aligned} \tag{24}$$

where (23) is exploited in the first equality and (21) in the second equality. The derivative vanishes $\frac{\mathrm{d}^k}{\mathrm{d}t^k} P_n\big(\gamma_t\big) = 0$ for $k \geq 2n + 1$.

7. REFERENCES

[1] Earl G Williams, *Fourier Acoustics: Sound Radiation and Nearfield Acoustical Holography*, Academic Press, London, UK, 1999.

[2] Nail A Gumerov and Ramani Duraiswami, *Fast Multipole Methods for the Helmholtz Equation in Three Dimensions*, Elsevier, Oxford, UK, 2005.

[3] Jens Ahrens, *Analytic Methods of Sound Field Synthesis*, Springer, Berlin, Germany, 2012.

[4] Boaz Rafaely, *Fundamentals of Spherical Array Processing*, Springer, Berlin, Germany, 2nd edition, 2019.

[5] Franz Zotter and Matthias Frank, *Ambisonics*, Springer, Cham, Switzerland, 2019.

[6] Jens Ahrens and Sascha Spors, "An analytical approach to sound field reproduction with a movable sweet spot using circular distributions of loudspeakers," in *Proc. Int. Conf. Acoust. Speech Signal Process. (ICASSP)*, Taipei, Taiwan, 2009, pp. 273–276.

[7] Nara Hahn, Fiete Winter, and Sascha Spors, "Local wave field synthesis by spatial band-limitation in the circular/spherical harmonics domain," in *Proc. Audio Eng. Soc. (AES) Conv.*, Paris, France, May 2016, pp. 1–12.

[8] Nara Hahn, Frank Schultz, and Sascha Spors, "Cylindrical radial filter design with application to local wave field synthesis," *J. Audio Eng. Soc. (JAES)*, in press.

[9] Hannes Pomberger, "Angular and radial directivity control for spherical loudspeaker arrays," M.S. thesis, University of Music and Performing Arts, Graz, Austria, 2008.

[10] Sascha Spors, Vincent Kuscher, and Jens Ahrens, "Efficient realization of model-based rendering for 2.5-dimensional near-field compensated higher order Ambisonics," in *Proc. Workshop Appl. Signal Process. Audio Acoust. (WASPAA)*, New Paltz, USA, Oct. 2011, pp. 61–64.

[11] Stefan Lösler and Franz Zotter, "Comprehensive radial filter design for practical higher-order Ambisonic recording," in *Proc. 41st German Annu. Conf. Acoust. (DAGA)*, 2015, pp. 452–455.

[12] Mark Poletti, Thushara D Abhayapala, and Paul D Teal, "Time domain description of spatial modes of 2D and 3D free-space Greens functions," in *Proc. Audio Eng. Soc. (AES) Conf.*, Guildford, UK, 2016, pp. 1–9.

[13] Fei Ma, Wen Zhang, and Thushara D Abhayapala, "Reference signal generation for broadband ANC systems in reverberant rooms," in *Proc. Int. Conf. Acoust. Speech Signal Process. (ICASSP)*, Calgary, Canada, 2018, pp. 216–220.

[14] Huiyuan Sun, Thushara D Abhayapala, and Prasanga N Samarasinghe, "Time domain spherical harmonic analysis for adaptive noise cancellation over a spatial region," in *Proc. Int. Conf. Acoust. Speech Sig. Process. (ICASSP)*, 2019, pp. 516–520.

[15] Nara Hahn, Fiete Winter, and Sascha Spors, "2.5D local wave field synthesis of a virtual plane wave using a time domain representation of spherical harmonics expansion," in *Proc. 23rd Int. Cong. Acoust. (ICA)*, Aachen, Germany, Sept. 2019, pp. 1132–1139.

[16] O Merih Buyukdura and S Sencer Koc, "Two alternative expressions for the spherical wave expansion of the time domain scalar free-space Green's function and an application: Scattering by a soft sphere," *J. Acoust. Soc. Am. (JASA)*, vol. 101, no. 1, pp. 87–91, 1997.

[17] Nara Hahn and Sascha Spors, "Time-domain representations of a plane wave with spatial band-limitation in the spherical harmonics domain," in *Proc. 45th German Annu. Conf. Acoust. (DAGA)*, Rostock, Germany, Mar. 2019, pp. 1434–1439.

[18] Nara Hahn, Frank Schultz, and Sascha Spors, "Time domain sampling of the radial functions in spherical harmonics expansions," *IEEE Trans. Signal Process.*, vol. 69, pp. 4502–4512, 2021.

[19] Nara Hahn and Sascha Spors, "Discrete time modeling of spherical harmonics expansion by using band-limited step functions," in *Proc. 46th German Annu. Conf. Acoust. (DAGA)*, Hannover, Germany, Mar. 2020, pp. 1188–1191.

[20] Nara Hahn, Frank Schultz, and Sascha Spors, "Higher order antiderivatives of band limited step functions for the design of radial filters in spherical harmonics expansions," in *Proc. 24th Int. Conf. Digital Audio Effects (DAFx)*, Online, Sept. 2021, pp. 184–190.

[21] Vesa Välimäki, Jussi Pekonen, and Juhan Nam, "Perceptually informed synthesis of bandlimited classical waveforms using integrated polynomial interpolation," *J. Acoust. Soc. Am. (JASA)*, vol. 131, no. 1, pp. 974–986, 2012.

[22] Fabián Esqueda, Vesa Välimäki, and Stefan Bilbao, "Antialiased soft clipping using an integrated bandlimited ramp," in *Proc. 24th Eur. Signal Process. Conf. (EUSIPCO)*, Budapest, Hungary, 2016, pp. 1043–1047.

[23] Fabián Esqueda, Stefan Bilbao, and Vesa Välimäki, "Aliasing reduction in clipped signals," *IEEE Trans. Signal Process.*, vol. 64, no. 20, pp. 5255–5267, 2016.

[24] Frank W. J. Olver, Daniel W. Lozier, Ronald F. Boisvert, and Charles W. Clark, *NIST Handbook of Mathematical Functions Handback*, Cambridge University Press, New York, NY, USA, 2010.

[25] Jie Li and Balasubramaniam Shanker, "Time-dependent Debye-Mie series solutions for electromagnetic scattering," *IEEE Trans. Antennas Propag.*, vol. 63, no. 8, pp. 3644–3653, 2015.

[26] Francesco Faá di Bruno, "Sullo sviluppo delle funzioni," *Annali di Scienze Matematiche e Fisiche*, vol. 6, pp. 479–480, 1855.

[27] Andreas Franck and Karlheinz Brandenburg, "A closed-form description for the continuous frequency response of Lagrange interpolators," *IEEE Sig. Process. Lett.*, vol. 16, no. 7, pp. 612–615, 2009.

[28] Vesa Välimäki, *Discrete-Time Modeling of Acoustic Tubes Using Fractional Delay Filters*, Ph.D. thesis, Helsinki University of Technology, Espoo, Finland, 1995.

[29] Louis François Antoine Arbogast, *Du calcul des dérivations*, Levrault, Strasbourg, France, 1800.